BNL-223669-2022-JAAM

Highly Selective Methane to Methanol Conversion on Inverse SnO2/ Cu2O/Cu(111) Catalysts: Unique Properties of SnO2 Nanostructures and the Inhibition of the Direct Oxidative Combustion of Methane

E. Huang, P. Liu

To be published in "ACS CATALYSIS"

September 2022

Chemistry Department

Brookhaven National Laboratory

U.S. Department of Energy

USDOE Office of Science (SC), Basic Energy Sciences (BES) (SC-22)

DISCLAIMER

Highly Selective Methane to Methanol Conversion on Inverse $SnO_2/Cu_2O/Cu(111)$ Catalysts: Unique Properties of SnO_2 Nanostructures and the Inhibition of the Direct Oxidative Combustion of Methane

Erwei Huang[1,#], Ning Rui[2,#], Rina Rosales[1], Jindong Kang[1], Slavomir Nemšák[3], Sanjaya D. Senanayake[2], José A. Rodriguez[1,2,*], Ping Liu[1,2,*]

[1] Department of Chemistry, Stony Brook University, Stony Brook, NY 11794, (USA)

[2] Chemistry Division, Brookhaven National Laboratory, Upton, NY 11973, (USA)

3 Advanced Light Source, Lawrence Berkeley National Laboratory, Berkeley, CA 94720, (USA)

[*] Corresponding authors: rodrigez@bnl.gov (J.A.R.), pingliu3@bnl.gov (P. L.)

[#] E.H. and N.R. contributed in equal terms to this research.

Abstract

Direct methane to methanol ($CH_4 \rightarrow CH_3OH$) conversion in heterogeneous catalysis has been a long-standing challenge due to the difficulties in equalizing the activation of methane and protection of the methanol product at the same reaction conditions. Here, we report an inverse catalyst, consisting of small structures of SnO_2 (0.5-1 nm in size) dispersed on Cu_2O/Cu(111), for highly selective CH_3OH production from CH_4. This system was investigated by combining theoretical [density functional theory calculations (DFT), kinetic Monte Carlo simulations (KMC)] and experimental methods [scanning tunneling microscopy (STM), ambient-pressure X-ray photoelectron spectroscopy (AP-XPS)]. The DFT and AP-XPS studies showed that on SnO_2/Cu_2O/Cu(111) the conversion of CH_4 by oxygen (O_2) preferred complete combustion to carbon dioxide (CO_2). The addition of water (H_2O) enhanced the production of CH_3OH to nearly 100% selectivity in KMC simulations. This trend was consistent with results of AP-XPS. The presence of water in the reaction environment rendered an extremely high amount of methoxy species (*CH_3O), a precursor for CH_3OH production. The high CH_3OH selectivity of SnO_2/Cu_2O/Cu(111) reflected the unique atomic and electronic structure of the supported SnO_2 nanoparticles. As a result, the O_2 adsorption and dissociation, and thus the full combustion of CH_4 to CO_2, was completely suppressed; while the H_2O dissociative adsorption was still feasible, providing active hydroxyl species for a truly selective CH_4 to CH_3OH conversion.

Keywords: Tin oxide, copper oxide, selective methane conversion, methanol selectivity, inverse catalysts

1. Introduction

The direct transformation of methane (CH_4) to commodity chemicals has attracted strong interests due to the abundancy of natural gas and its potential impact on diminishing the greenhouse effect[1-4]. One of the most promising processes is the direct methane oxidation to methanol ($CH_4 + 0.5\ O_2 \rightarrow CH_3OH$), which only requires to break one C-H bond and insert another oxygen atom through a rebound [5] or concerted mechanism[6]. Achieving this process could enable an efficient utilization of natural gas resources and contribute to a methanol-based economy[7, 8]. However, this process has long been challenging due to the prevalence of two critical cofactors, a highly stable CH_4 reactant that requires high temperature to activate and a reactive CH_3OH product that needs mild environments to remain intact and not decompose[9-12]. Nature has addressed this challenge by employing enzymes that achieve a direct $CH_4 \rightarrow CH_3OH$ conversion at room temperature with very high selectivity and efficiency[13-17]. In addition, similar processes have been observed in another type of systems, zeolites, that have active chemistry due to their cage features and can stabilize active metal cation sites similar to those seen in the enzyme catalysts[18-21].

Recently, the activation of CH_4 has been achieved at mild temperatures over well-defined metal oxides and complex interfaces[22-26]. However, such systems are typically too active, decomposing the formed CH_3OH[27, 28]. One way to balance the activation of CH_4 and the preservation of the generated CH_3OH is to add water (H_2O) into the reaction environment[27-30]. The H_2O can not only block extremely reactive sites and passivate the decomposition of CH_3OH, but also facilitate methanol production by directly participating in the $CH_4 \rightarrow CH_3OH$ process and being involved in the final extraction step of the adsorbed methoxy ($*CH_3O$) or $*CH_3OH$[29, 30].

Here, we examined the reaction of CH_4/O_2 and $CH_4/O_2/H_2O$ mixtures on a typical inverse model catalyst that contains small particles of SnO_2 (0.5-1 nm in size, see Figure 1) dispersed on

Cu_2O/Cu(111), or SnO_2/Cu_2O/Cu(111) inverse catalyst in our notation.[24] Inverse catalysts generally consist of oxide nanoparticles supported on metal substrates[31-33]. These oxide nanoparticles can exhibit physical and chemical properties not seen in bulk oxides. Different from conventional oxide-supported metal catalysts, the inverse systems describe well the importance of oxide nanostructures in strong interaction with the metal component, being able to generate unique catalytic performance for the water-gas shift reaction[34-36], carbon monoxide (CO) oxidation[34, 37-39], carbon dioxide (CO_2) hydrogenation[34, 40-42], selective CH_4 conversion[28-30], and other processes[34, 43, 44]. Furthermore, the inverse catalysts also allow a close interplay of experimental measurements using surface science tools and theoretical studies. In this work, the inverse SnO_2/Cu_2O/Cu(111) model catalyst was utilized to explore its catalytic behaviors in selective CH_4 to CH_3OH conversion in consideration of the fact that SnO_x is often used as a gas sensor material for methane detection[45]. In addition, SnO_2/Cu_2O/Cu(111) is attractive due to the small particle size

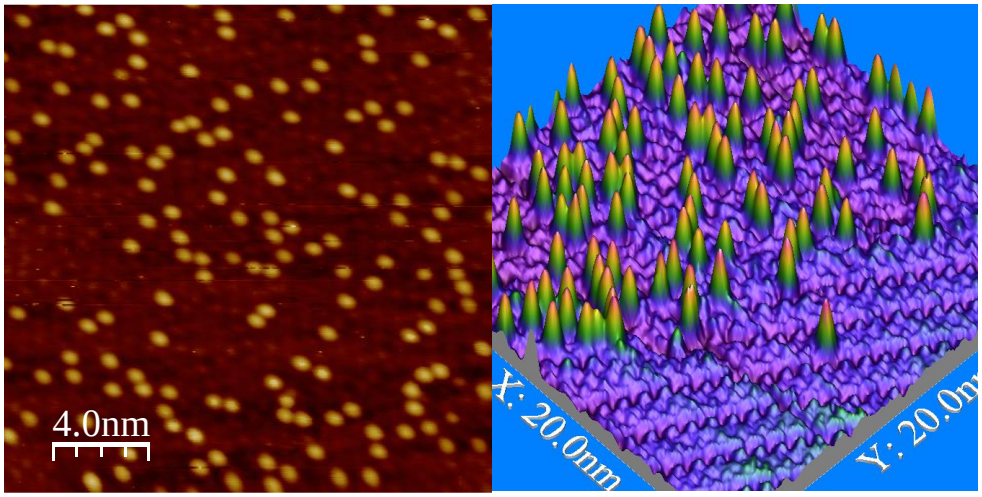

Figure 1. Two (left-side) and three (right-side) dimensional views of 0.2 monolayer (ML) of SnO_2 dispersed on a Cu_2O/Cu(111) surface, the scale of both images is 20 × 20 nm^2. The SnO_2/Cu_2O/Cu(111) system was prepared as described previously[24].

of SnO_2 and well dispersion over the oxide overlayer, not seen in the case of $ZnO/Cu_2O/Cu(111)$ and $CeO_2/Cu_2O/Cu(111)$ inverse catalysts previously investigated for the conversion of $CH_4 \rightarrow CH_3OH$[28,30].

The inverse $SnO_2/Cu_2O/Cu(111)$ catalyst was previously found to be able to activate CH_4 at room temperature due to its specific bridge Sn^{4+}-O-Sn^{2+} active sites[24]. Here, the results of calculations based on density functional theory (DFT) and kinetic Monte Carlo (KMC) simulations predict that that these motifs can enable a highly selective $CH_4 \rightarrow CO_2$ conversion upon exposure to O_2 and $CH_4 \rightarrow CH_3OH$ conversion with addition of H_2O. This theoretical prediction is in good agreement with the ambient-pressure X-ray photoelectron spectroscopy (AP-XPS) measurements, showing that the surface $*CH_x$ species can be completely transformed to $*CH_3O$ species upon the addition of H_2O, a key factor that correlate with the CH_3OH selectivity[29]. Such H_2O-promoted CH_3OH selectivity has also been observed previously for $CeO_2/Cu_2O/Cu(111)$ and $ZnO/Cu_2O/Cu(111)$ catalysts[29, 30], while it is more significant on $SnO_2/Cu_2O/Cu(111)$. From the results of the DFT calculations, the high CH_3OH selectivity with exposure to $CH_4/O_2/H_2O$ reflects the unique structure of the supported SnO_2 systems. Different from the $Cu_2O/Cu(111)$ supported CeO_2 and ZnO nanostructures[29, 30], such SnO_x moiety upon interaction with CuO_x can completely suppress the adsorption and dissociation of O_2, which leads to the full combustion of CH_4 to CO_2, but still enabling the H_2O dissociative adsorption to provide active *OH species for the selective CH_4 partial oxidation to CH_3OH.

2. Results and discussion:

2.1 DFT calculations for CH_4, O_2 and H_2O interactions on $SnO_2/Cu_2O/Cu(111)$

Our previous studies identified the facile activation of CH_4 on $SnO_2/Cu_2O/Cu(111)$ surfaces, suggesting their potential use as catalysts for the partial oxidation of CH_4 to CH_3OH[24]. To test this hypothesis, in this work DFT calculations were performed to identify the potential catalytic behavior of $SnO_2/Cu_2O/Cu(111)$ catalysts using a $Sn_3O_6/Cu_2O/Cu(111)$ model (Figure S1), which described well the structures observed experimentally[24].

CH_4, O_2 and H_2O molecules were first used as probe molecules over the $SnO_2/Cu_2O/Cu(111)$ surfaces and each exhibited a unique behavior (Figure 2). The SnO_2-Cu_2O interface binds CH_4 weakly, with an adsorption energy (E_{ads}) of -0.69 kcal/mol; yet the C-H bond cleavage can proceed with a moderate a barrier (E_a) of 22.14 kcal/mol[24]. While H_2O preferentially adsorbs at the interface (E_{ads} = -11.53 kcal/mol) and dissociates easily to an interfacial hydroxyl species (*OH), with a low barrier (E_a= 1.15 kcal/mol) through an exothermic process (ΔE = -15.22 kcal/mol), as shown in Figure 2. Such preferential H_2O adsorption and dissociation over CH_4 has been observed on the interfaces of Ce_3O_6-Cu_2O for description of $CeO_2/Cu_2O/Cu(111)$ (E_{ads} = -15.91 kcal/mol, E_a = 0.00 kcal/mol) and Zn_3O_3-Cu_2O for description of $ZnO/Cu_2O/Cu(111)$ (E_{ads} = -12.22 kcal/mol, E_a = 0.00 kcal/mol) catalysts[29, 30].

Limited catalytic activity is seen on $SnO_2/Cu_2O/Cu(111)$ towards the activation of the O_2 molecule, which corresponds to a weak adsorption (E_{ads} = -1.15 kcal/mol) and highly endothermic O-O bond cleavage (ΔE = 32.74 kcal/mol). In comparison with CeO_2-Cu_2O (E_{ads} = -14.53 kcal/mol, E_a = 5.54 kcal/mol) and ZnO-Cu_2O (E_{ads} = -5.77 kcal/mol, E_a = 10.61 kcal/mol)[29, 30], SnO_2-Cu_2O exhibits a much lower activity toward O_2 activation, which can lead to different catalytic performance for CH_4 conversion as demonstrated below by DFT, KMC and AP-XPS studies.

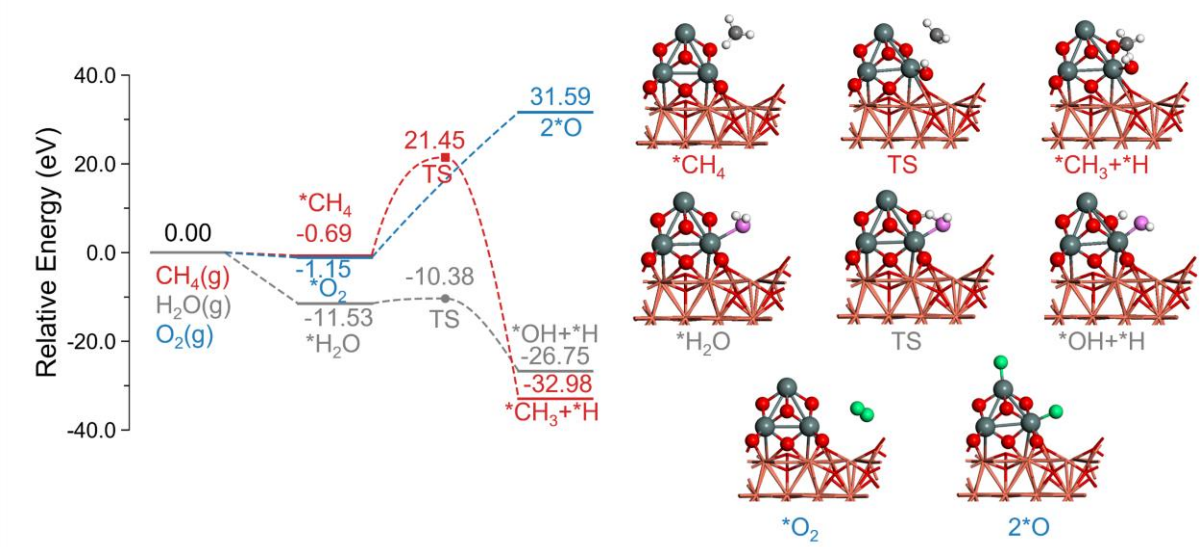

Figure 2: DFT-calculated potential energy diagram for CH_4, O_2 and H_2O adsorption and dissociation on the $Sn_3O_6/Cu_2O/Cu(111)$ model and the corresponding optimized structures of intermediates and transition states (TS) on the $Sn_3O_6/Cu_2O/Cu(111)$ system; Detailed structures for each of the three models are displayed in Figure S2. Dark green: Sn; brown: Cu; red: O in $SnO_2/Cu_2O/Cu(111)$; Green: O from O_2; Purple: O from H_2O; gray: C; white: H.

2.2 DFT and KMC studies for methane conversion on $SnO_2/Cu_2O/Cu(111)$ by O_2.

Previously, the facile CH_4 oxidation by O_2 at the interfaces of CeO_2-$Cu_2O/Cu(111)$ and ZnO-$Cu_2O/Cu(111)$ was observed and mainly ascribed to generation of interfacial *O species, which led to the complete combustion of CH_4 to CO_2[29, 30]. However, this is not the case for $SnO_2/Cu_2O/Cu(111)$. Due to the weak interaction between O_2 and SnO_2-Cu_2O interface, there is no adsorption of O_2 and thus no formation of interfacial *O species. Instead, as shown in Figure 3, CH_4 dissociates at the interface of SnO_2-Cu_2O, which further dehydrogenates to $*CH_2$ (ΔE = 2.31 kcal/mol, E_a = 30.67 kcal/mol) and *CH (ΔE = 8.07 kcal/mol, E_a = 25.60 kcal/mol) species. Here,

the dehydrogenated *H fragments likely reduce the $SnO_2/Cu_2O/Cu(111)$ catalyst by forming an oxygen vacancy ($*O_v$) site. In this case, O_2 helps to fill the $*O_v$ site via strong adsorption (E_{ads} =

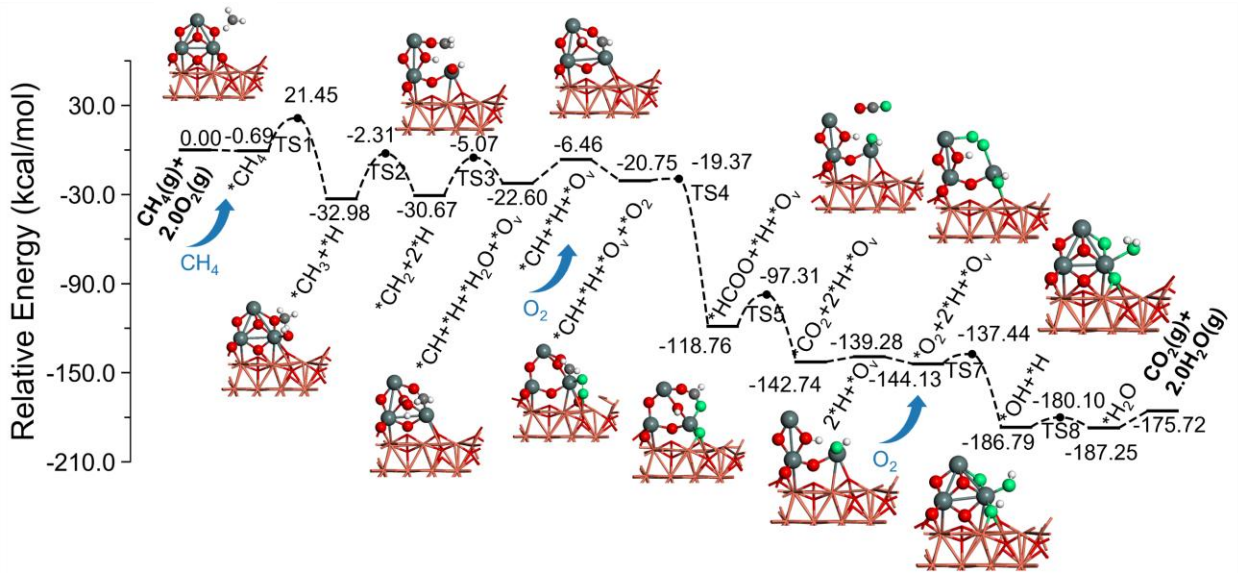

Figure 3: DFT-calculated potential energy diagram for CH_4 oxidation on a $Sn_3O_6/Cu_2O/Cu(111)$ substrate under CH_4/O_2 mixtures and the corresponding geometries of key intermediates in the reaction, also see Figure S3 for detailed geometries of all the intermediates and transition states. Dark green: Sn; brown: Cu; red: O in $SnO_2/Cu_2O/Cu(111)$; Green: O from O_2; gray: C; white: H.

-19.83 kcal/mol) and favorable dissociation (ΔE = -11.99 kcal/mol, E_a = 18.45 kcal/mol), enabling the facile oxidation of *CH to *HCOO species (E_a =1.38 kcal/mol, ΔE = -98.01 kcal/mol) and eventually the formation of $*CO_2$ species (ΔE = -23.98 kcal/mol, E_a = 21.45 kcal/mol). In addition, the facile O_2 dissociation at the $*O_v$ site also facilitate the removal of the dissociated *H species in the form of H_2O (ΔE = -42.67 kcal/mol, E_a = 6.68 kcal/mol, Figure 3). During the combustion process, the most difficult elementary step is likely the dehydrogenation of $*CH_3$ to $*CH_2$ with the highest barrier of 30.67 kcal/mol.

The KMC simulations were performed based on the DFT calculated barriers and pre-exponential factors (see Figure S4, Tables S1 and S2, also see computational methods for details), under a CH_4/O_2 ratio of 2:1 at 450K. The results showed that the conversion rate of CH_4 (1.02×10^{12} molecules cm^{-2} s^{-1}) at steady state is not as fast as that on $CeO_2/Cu_2O/Cu(111)$ (1.10×10^{17} molecules cm^{-2} s^{-1}) and $ZnO/Cu_2O/Cu(111)$ (3.04×10^{14} molecules cm^{-2} s^{-1}) under the same conditions (Figure S5). This is associated with the suppressed O_2 dissociation and thus lack of interfacial *O species, which was previously found to facilitate the first C-H bond breaking of CH_4 and the sequential dehydrogenation process, e.g. $*CH_3 \rightarrow *CH_2$[29, 30]. In term of selectivity, only CO_2 was observed on $SnO_2/Cu_2O/Cu(111)$; while trace amount of CH_3OH was seen for $CeO_2/Cu_2O/Cu(111)$ and ~ 60% of selectivity was achieved on $ZnO/Cu_2O/Cu(111)$ (Figure 4a). The standout high CH_3OH selectivity at the ZnO-Cu_2O interface was mainly ascribed to its unique balance among the processes of CH_3OH formation, desorption, and decomposition by the ZnO-Cu_2O interface, as demonstrated previously[30]. Although both $SnO_2/Cu_2O/Cu(111)$ and $CeO_2/Cu_2O/Cu(111)$ are not selective to CH_3OH when CH_4 is oxidized by O_2, the origin behind is not the same. The CeO_2-Cu_2O interface is too active to prevent the decomposition of $*CH_3OH$ species formed at the active interfacial *O sites via the $*CH_4+*O \rightarrow *CH_3OH$[29] process, while there is barely any O_2 dissociation observed at the SnO_2-Cu_2O interface and thus no direct formation of $*CH_3OH$ over $SnO_2/Cu_2O/Cu(111)$ is observed. Finally, at the KMC-simulated steady-state, the catalysts are stable, where only small amount of $*CH_3$, *OH and trace of $*CH_2$ species were observed at $SnO_2/Cu_2O/Cu(111)$ surface (Figures 4b and S6) as seen for $CeO_2/Cu_2O/Cu(111)$ and $ZnO/Cu_2O/Cu(111)$ catalysts[29, 30].

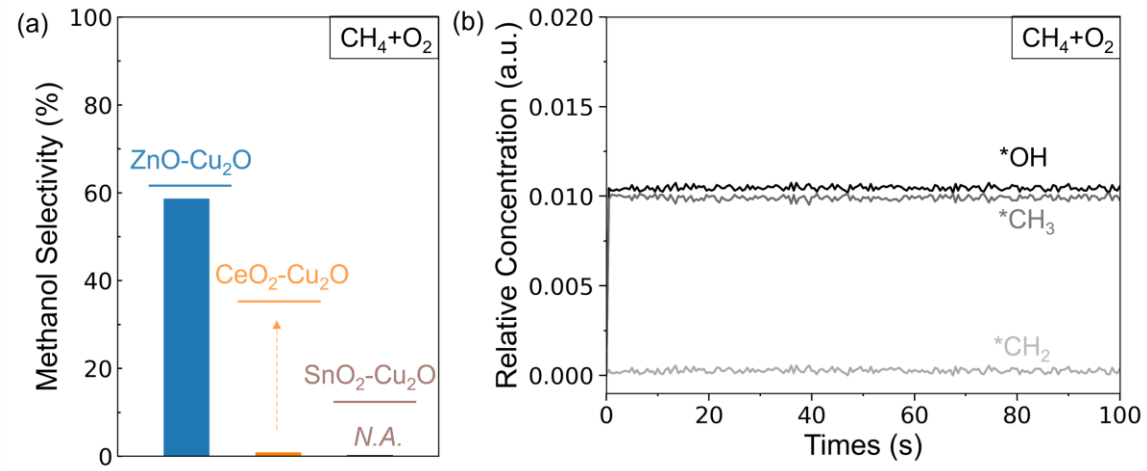

Figure 4: (a) KMC-simulated methanol production selectivity over the interfaces of $ZnO/Cu_2O/Cu(111)$, $CeO_2/Cu_2O/Cu(111)$ and $SnO_2/Cu_2O/Cu(111)$ catalysts and (b) KMC-simulated relative concentrations of surface species on $SnO_2/Cu_2O/Cu(11)$ catalysts on exposure to a gas mixture of CH_4 and O_2 with a pressure ratio of 2:1 at 450K.

Overall, the presence of O_2 helps in filling the surface $*O_v$ and removing *H species formed during CH_4 combustion on $SnO_2/Cu_2O/Cu(111)$, similar to the cases of $CeO_2/Cu_2O/Cu(111)$ and $ZnO/Cu_2O/Cu(111)$ catalysts. Differently, in the cases of $CeO_2/Cu_2O/Cu(111)$ and $ZnO/Cu_2O/Cu(111)$, the facile O_2 dissociation facilitates the first C-H bond cleavage of CH_4 through the formation of an interfacial *O species [29, 30]. On $SnO_2/Cu_2O/Cu(111)$, on the other hand, O_2 participates in the reaction only when the $*O_v$ is generated, enabling the oxidation of *CH species to *HCOO and its selective conversion to CO_2.

2.3 DFT and KMC studies for methane conversion on $SnO_2/Cu_2O/Cu(111)$ by O_2/H_2O.

Water has been found to play a key role in the $CH_4 \rightarrow CH_3OH$ conversion process by enzymes, metal-exchanged zeolites[18, 19, 46], and oxide/metal catalysts[27-30]. Thus, we further studied the effects for CH_4 conversion upon the addition of H_2O into O_2 environments. As shown in Figure

2, H_2O preferentially adsorbs at the interface of $SnO_2/Cu_2O/Cu(111)$ catalysts, blocking the site for the direct interaction with $*CH_4$ as reported previously for other oxide-oxide interfaces[27-30]. Moreover, the resulted interfacial *OH species also promotes the selective $CH_4 \rightarrow CH_3OH$ conversion through the $*OH+*CH_4 \rightarrow *CH_3OH+*H$ process (ΔE = -18.68 kcal/mol, E_a = 23.06 kcal/mol, Figure 5 and Figure S7). Wherein the corresponding barrier is slightly higher than that on $CeO_2/Cu_2O/Cu(111)$ (E_a = 22.37 kcal/mol) and lower than the one on $ZnO/Cu_2O/Cu(111)$ (E_a

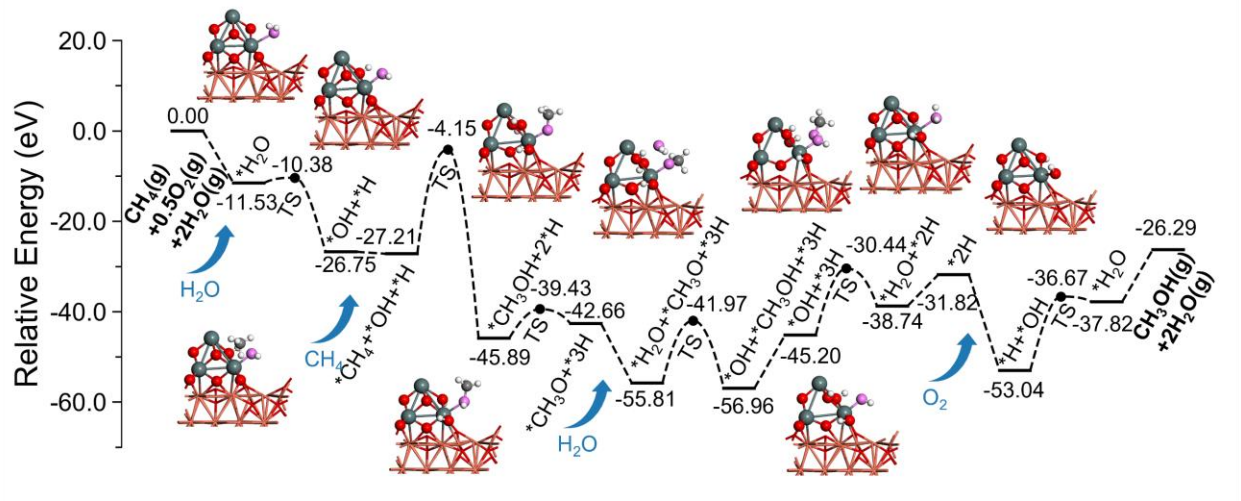

Figure 5: DFT-calculated potential energy diagram for CH_4 oxidation by interfacial *OH species dissociated from $*H_2O$ on $Sn_3O_6/Cu_2O/Cu(111)$ model and the corresponding structures for selected intermediates, also see Figure S7 for detailed structures of all intermediates and transition states. Dark green: Sn; brown: Cu; red: O in $SnO_2/Cu_2O/Cu(111)$; Purple: O from H_2O; gray: C; white: H.

= 25.82 kcal/mol)[29, 30]. The formed $*CH_3OH$ species at the SnO_2-Cu_2O interface either desorbs to gas phase (ΔE = 12.45 kcal/mol) or dissociates into $*CH_3O$ species (ΔE = 6.46 kcal/mol, E_a = 3.23 kcal/mol). With the presence of H_2O in the reaction environment, the formed $*CH_3O$ species can be stabilized (ΔE = -13.84 kcal/mol) and easily extracted in the form of $*CH_3OH$ through an

$CH_3O\cdots HOH$ motif (ΔE = -1.15 kcal/mol, E_a = 13.84 kcal/mol). A similar behavior has been observed on both $CeO_2/Cu_2O/Cu(111)$ and $ZnO/Cu_2O/Cu(111)$ catalysts[29, 30]. During the process, as seen for the $CeO_2/Cu_2O/Cu(111)$ and $ZnO/Cu_2O/Cu(111)$ systems,[29, 30] O_2 also contributes to stabilize the $SnO_2/Cu_2O/Cu(111)$ catalyst by filling the $*O_v$ sites generated by removal of the surface *H species in the form of H_2O (Figure 5).

Under the steady-state conditions of the KMC simulation at 450 K with a gas mixture of $CH_4/O_2/H_2O$ at a ratio of 2:1:4, the SnO_2-Cu_2O interface exhibits an adequate CH_4 conversion rate (6.69×10^{15} molecules cm^{-2} s^{-1}), being twice more active than $ZnO/Cu_2O/Cu(111)$ (2.76×10^{15} molecules cm^{-2} s^{-1}) (Figure 6a), but less active in the reaction with O_2 only (Figure 4a). In both cases, $CeO_2/Cu_2O/Cu(111)$ remains as the most active (3.90×10^{17} molecules cm^{-2} s^{-1}) among the three systems (Figure S8). Such trend can be well described by the corresponding activation energy for the $*OH+*CH_4 \rightarrow *CH_3OH+*H$ step, which also shows an increase in the sequence: CeO_2 < SnO_2 < ZnO. More importantly, with the presence of H_2O, $SnO_2/Cu_2O/Cu(111)$ becomes the best system for the production of CH_3OH, with a selectivity close to 100%, followed by $ZnO/Cu_2O/Cu(111)$ and $CeO_2/Cu_2O/Cu(111)$ in a decreasing sequence (Figure 6a). This is a completely opposite trend in comparison to the case without H_2O, which barely produces CH_3OH (Figure 4a). Furthermore, the addition of H_2O also promotes the conversion of the surface $*CH_x$ species to $*CH_3O$ and increases the coverage of surface*OH species (Figures 6b and S9), which are necessary to enable the high CH_3OH selectivity[27-30].

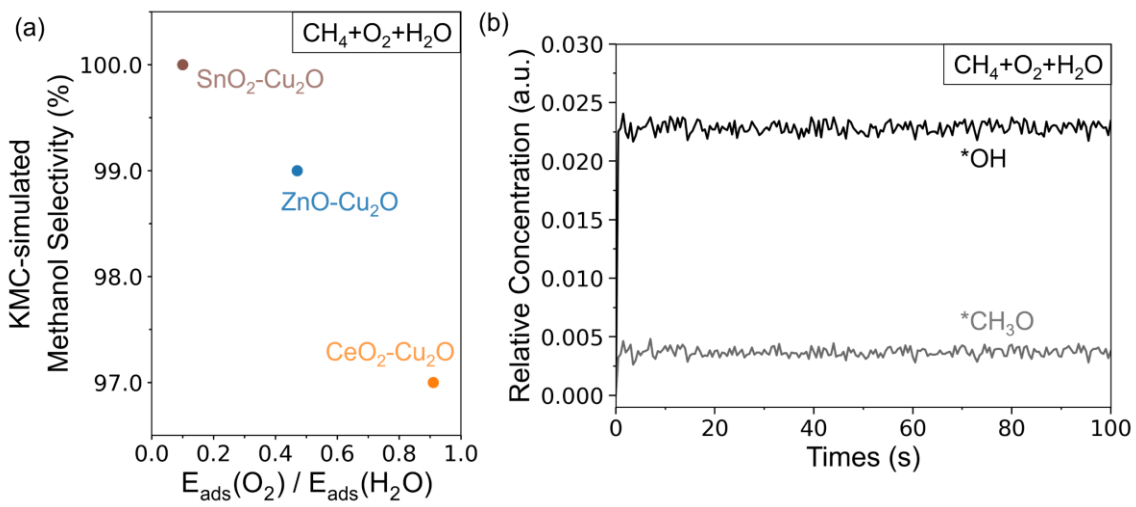

Figure 6: (a) KMC-simulated methanol production selectivity over the interfaces of $ZnO/Cu_2O/Cu(111)$, $CeO_2/Cu_2O/Cu(111)$ and $SnO_2/Cu_2O/Cu(111)$ catalysts and its corresponding correlations with the ratio of O_2/H_2O binding energy, $E_{ads}(O_2)/E_{ads}(H_2O)$, the methanol selectivity was rounded down to the nearest integer. (b) KMC-simulated relative concentrations of surface species on $SnO_2/Cu_2O/Cu(11)$ catalysts on exposure to a gas mixture of CH_4, O_2 and H_2O with a pressure ratio of 2:1:4 at 450K.

The H_2O-induced increase in CH_4 conversion rate and selectivity tuning toward CH_3OH is mainly due to a completely altered reaction pathway for CH_4 conversion. As observed on both $CeO_2/Cu_2O/Cu(111)$ and $ZnO/Cu_2O/Cu(111)$ catalysts[29, 30], firstly the addition of H_2O not only blocks the active sites at the SnO_2-Cu_2O interface that enable the complete combustion of CH_4 to CO_2, but also generates a new active interfacial *OH species that can reform CH_4 directly to CH_3OH. Furthermore, the extraction of surface $*CH_3O$ species by the surrounding H_2O is also a key factor toward the high CH_3OH selectivity. Different from $CeO_2/Cu_2O/Cu(111)$ and $ZnO/Cu_2O/Cu(111)$ catalysts[29, 30], $SnO_2/Cu_2O/Cu(111)$ represents the extreme case, where the CH_4 undergoes the full combustion to CO_2 on exposure to O_2 and completely partial oxidation to

CH_3OH with the additional water; while for the other two systems CO_2 and CH_3OH always coexist at different ratios under the same conditions.

Interestingly, the CH_3OH selectivity likely depends on the ratio of O_2/H_2O adsorption energy ($E_{ads}(O_2)/E_{ads}(H_2O)$) at the MO_x-Cu_2O interfaces (Figure 6a). Specifically, the interface, which selectively binds O_2 weakly and H_2O strongly as seen for SnO_2-Cu_2O, can enable the high CH_3OH selectivity on exposure to the gas mixture of $CH_4/O_2/H_2O$. We note that $E_{ads}(O_2)/E_{ads}(H_2O)$ may be considered as a descriptor for the CH_3OH selectivity during the direct $CH_4 \rightarrow CH_3OH$ conversion, which can open a new catalyst design strategy. Yet, the data points here are limited, and further confirmation based on wider range of systems is necessary.

2.4 XPS studies for methane conversion on $SnO_2/Cu_2O/Cu(111)$ surfaces by O_2/H_2O.

The AP-XPS was also carried out to confirm the DFT/KMC-predicted catalytic behaviors of $SnO_2/Cu_2O/Cu(111)$ on interaction with $CH_4/O_2/H_2O$. As previously reported by our group, $SnO_2/Cu_2O/Cu(111)$ surfaces are very active towards CH_4 activation[24]. Methane undergoes dissociative adsorption ($CH_4 \rightarrow CH_x^* + (4 - x)H^*$) even at room temperature[24]. The facile CH_4 dissociation comes from a low activation barrier of 18.45~22.14 kcal/mol for C-H bond cleavage at the SnO_2-Cu_2O interface[24].

As demonstrated by the AP-XPS data in Figures 7 (C 1s) and S10 (O 1s), the addition of O_2 to CH_4 had a negligible impact on the type of surface species formed at room temperature. As in the case of CH_4 on $SnO_2/Cu_2O/Cu(111)$,[24] only CH_x groups were formed and no CH_xO species were detected under an environment of 10 mTorr O_2 and 20 mTorr CH_4, i.e. the stoichiometric ratio for the $CH_4 + 1/2O_2 \rightarrow CH_3OH$ reaction. At 400 K, the small $*CO_x$ peak at 288.9 eV was not observed for pure CH_4 on $SnO_2/Cu_2O/Cu(111)$[24] and could be the product of the full oxidation of the hydrocarbon by O adatoms produced by the dissociation of O_2.[30] This feature is much smaller

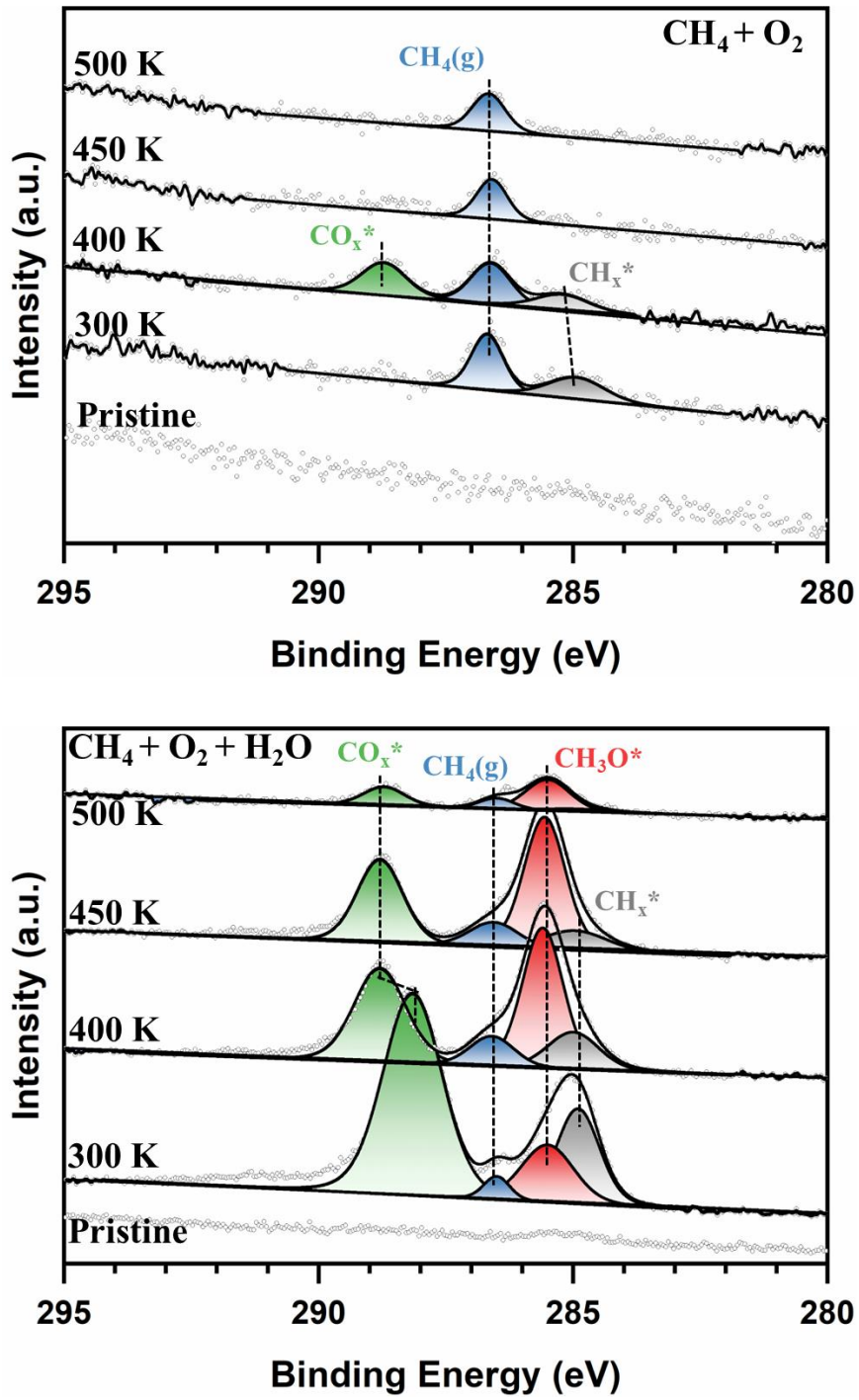

Figure 7 : Top: C 1s AP-XPS peaks of a 0.3 ML $SnO_2/Cu_2O/Cu(111)$ surface under 20 mTorr CH_4 + 10 mTorr O_2 at various temperatures. Bottom: Same XPS region for 0.3 ML $SnO_2/Cu_2O/Cu(111)$ under 20 mTorr CH_4 + 10 mTorr O_2 + 40 mTorr H_2O at various temperatures.

than that observed in AP-XPS after exposing $ZnO/Cu_2O/Cu(111)$ to $CH_4 + O_2$.[30] At higher temperatures of 450 and 500 K, only gaseous CH_4 was seen. It is also important to note that there are no signs of oxygenated species at these high temperatures. This result differs from $ZnO/Cu_2O/Cu(111)$ or $CeO_2/Cu_2O/Cu(111)$ surfaces, on which CH_4 can be effectively oxidized to $*CH_3O$ or CO_2.[29, 30] This suggests that the $SnO_2/Cu_2O/Cu(111)$ combination is essentially inert for the $CH_4 \rightarrow CH_3OH$ reaction, in accordance with the DFT and KMC results of Figures 3 and 4.

Upon the introduction of H_2O into the system at 300 K, the AP-XPS clearly show a new surface chemistry, bottom panel in Figure 7. At room temperature, we found that there is a ten-fold increase in the amount of CH_x* (284.6 eV) present. There are also clear peaks for intense $*CO_x$ and $*CH_3O$ species, which are completely absent in the water free case previously. Accordingly, the O1s data shown in Figure S10 also confirms the present of rich oxygenated species with the addition of water. When switching from a CH_4/O_2 reaction feed (top panel in Figure 8) to $CH_4/O_2/H_2O$ (bottom panel in Figure 8), heating to 400 or 450 K increased the concentration of $*CH_3O$ and decreased the $*CO_x$ and $*CH_3O$ signals. Thus, it appears that the addition of H_2O to the feed enables the effective CH_4 conversion on $SnO_2/Cu_2O/Cu(111)$ surfaces. This confirms the DFT-calculated result that H_2O can be easily dissociated at the SnO_2-Cu_2O interface to form *OH species, hence promoting the reforming of CH_4 (Figures 2 and 5).

A comparison of the behavior of reaction mixtures with ("wet" conditions) and without ("dry" conditions) the presence of water was further conducted to identify the *OH effects on the conversion of CH_4 over $SnO_2/Cu_2O/Cu(111)$ catalysts, see Figure 8. At 450 K, the difference between the wet and dry reaction is the most pronounced; whilst the dry reaction mixture has nothing except gaseous CH_4, the wet reaction set is rich in surface intermediates such as $*CO_x$,

*CH_3O and *CH_x. Taken together, at 450 K, the $SnO_2/Cu_2O/Cu(111)$ surface could activate CH_4 effectively, but the oxidation of CH_4 with O_2 to produce oxygenates is not feasible. However, when H_2O is added into the system, the production of *CH_3O is enhanced. These XPS observations are fully consistent with the DFT calculations and KMC simulations indicating that adsorbed *OH groups accelerate the CH_4 dissociation and participate in the formation of CH_3O* directly.

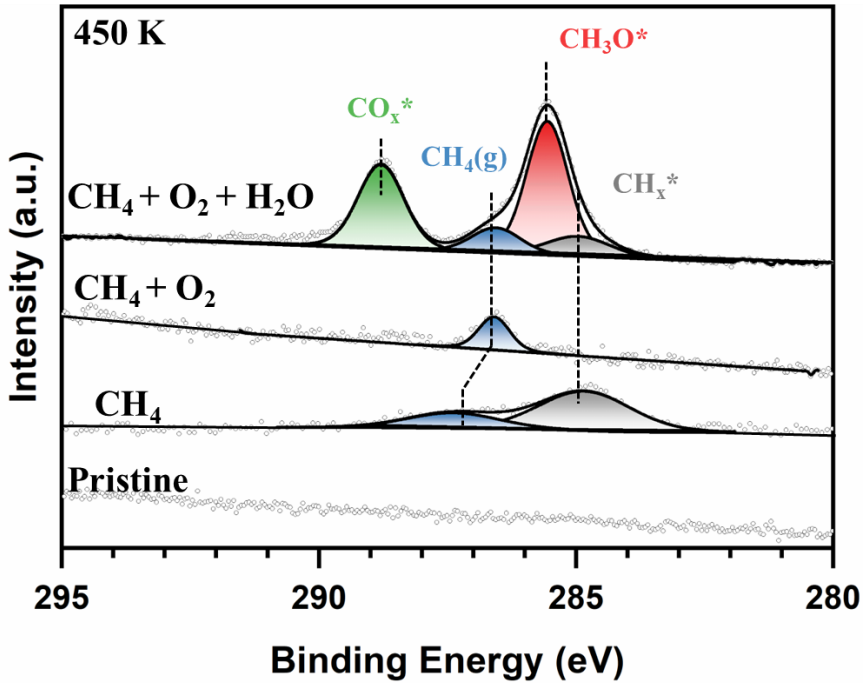

Figure 8: C 1s AP-XPS peaks of 0.3 ML $SnO_2/Cu_2O/Cu(111)$ surfaces under various conditions (20 mTor CH4; 20 mTorr CH_4 + 10 mTorr O_2; and 20 mTorr CH_4 + 10 mTorr O_2 + 40 mTorr H_2O) at 450 K. The data under 20mTorr of CH_4 is taken from ref[24].

The relative amount of *CH_3O detected by AP-XPS for three catalysts: $ZnO/Cu_2O/Cu(111)$, $CeO_2/Cu_2O/Cu(111)$, and $SnO_2/Cu_2O/Cu(111)$ were further compared (Figure 9). The relative *CH_3O concentration on $SnO_2/Cu_2O/Cu(111)$ surface is much higher than that on the $ZnO/Cu_2O/Cu(111)$ and $CeO_x/Cu_2O/Cu(111)$ surfaces. This is in line with the theoretical predictions that the $SnO_2/Cu_2O/Cu(111)$ has the highest CH_3OH selectivity during CH_4 conversion

by O_2 and H_2O (Figure 6a), following our previous study where a high concentration of surface *CH_3O species correlates with a high CH_3OH selectivity[29]. Note that the size of MO_x islands on the Cu_2O/Cu(111) substrate follows the trend of SnO_2[24] < CeO_2[35] < ZnO[47]. Among the three systems, the SnO_2 nanostructure is more uniformly dispersed and comprised of nanoparticles around 1 nm (Figure 1), which minimizes the possible decomposition of surface *CH_3O species on SnO_2/Cu_2O/Cu(111); while the full oxidation to CO_2 can always be observed in some degree for CeO_2/Cu_2O/Cu(111) and ZnO/Cu_2O/Cu(111) with larger islands on the surface with multiple active sites[30, 35]. The unique properties of atomic and electronic structure of highly dispersed SnO_2 nanoparticles also strongly contribute to the enriched CH_3O* concentration, as it will be discussed below.

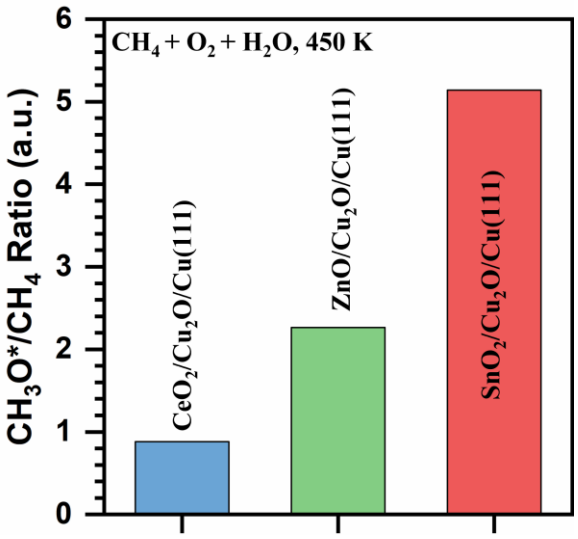

Figure 9: Comparison of the CH_3O*/CH_4 signal ratio for ZnO/Cu_2O/Cu(111), CeO_2/Cu_2O/Cu(111), and SnO_2/Cu_2O/Cu(111) catalysts. Reaction conditions: 20 mTorr CH_4 + 10 mTorr O_2 + 40 mTorr H_2O at 450 K. The data of ZnO/Cu_2O/Cu(111) and CeO_2/Cu_2O/Cu(111) were taken from ref [29, 30].

Overall, the AP-XPS measurements are fully consistent with theoretical predictions where the addition of H_2O helps to tune the CH_3OH production rate and selectivity during the conversion of CH_4 by O_2 due to the unique nanostructure provided by the SnO_2-Cu_2O interface[24]. In addition, the high relative concentration of $*CH_3O$ species on $SnO_2/Cu_2O/Cu(111)$ indicates that one could control the CH_3OH product selectivity by modifying different MO_x-Cu_2O interfaces and optimizing the special nanostructure metal oxide size to the potential uniform motif with the highest CH_3OH production selectivity.

2.5 Origin of the high CH_3OH selectivity over $SnO_2/Cu_2O/Cu(111)$.

The high CH_3OH selectivity of $SnO_2/Cu_2O/Cu(111)$ upon exposure to a $CH_4/O_2/H_2O$ mixture, observed both theoretically and experimentally, can be well associated with the unique atomic and electronic structure of the SnO_2-Cu_2O interface. This determines the binding to O_2/H_2O, which scales well with the CH_3OH selectivity (Figure 6a). Specifically, the coordination number of an interfacial Sn atom in $SnO_2/Cu_2O/Cu(111)$ is only 16.7% less than that of a Sn atom in bulk SnO_2 (Figure S11), which only renders a slight difference in the distribution/position of the Sn 5p levels according to the partial density of states (PDOS) (Figure 10). Upon interaction with the O_2 molecule, the electronic states barely changed due to the weak interaction between O_2 and SnO_2-Cu_2O interface (E_{ads} = -1.15 kcal/mol). A similar situation was also observed for $ZnO/Cu_2O/Cu(111)$ (Figures S11 and S12), and O_2 remains weakly bound (E_{ads} = -5.77 kcal/mol)). Yet, compared to Sn the reduction in coordination number going from bulk ZnO to interfacial Zn is slightly more (25.0%) and thus the binding of O_2 is slightly strengthened. However, that is not the case for $CeO_2/Cu_2O/Cu(111)$. The interfacial Ce atom on $Ce_3O_6/Cu_2O/Cu(111)$ is highly uncoordinated with the coordination number of about 50.0% less than that of the bulk CeO_2 (Figure S11). Such undercoordinated Ce atom at the CeO_2-Cu_2O interface is highly active in comparison

to its bulk state (Figure S13) by showing a partially occupied 4f states near the Fermi level, the fingerprint for reduction of Ce^{4+} to Ce^{3+} (E_{ads} = -14.53 kcal/mol).

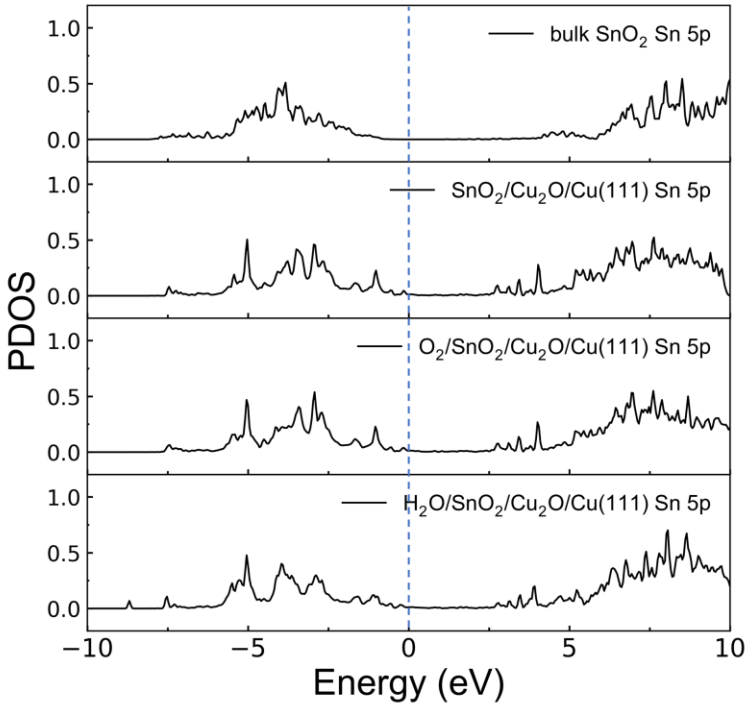

Figure 10: Partial density of states (PDOS) of Sn 5p levels for bulk SnO_2, $SnO_2/Cu_2O/Cu(111)$, $O_2/SnO_2/Cu_2O/Cu(111)$ and $H_2O/SnO_2/Cu_2O/Cu(111)$. The blue dashed line denotes for the Fermi level.

The three MO_x-Cu_2O interfaces also show similar trends for H_2O adsorption with -15.91 kcal/mol for $CeO_2/Cu_2O/Cu(111)$, -12.22 kcal/mol for $ZnO/Cu_2O/Cu(111)$ and -11.53 kcal/mol for $SnO_2/Cu_2O/Cu(111)$, in an increasing sequence; yet the difference from one system to the next is rather smaller than that for O_2 adsorption. Both O_2 and H_2O lead to a stabilization of the interfacial metal ions upon adsorption (Figures 10, S12 and S13). However, unlike O_2 adsorption, the H_2O adsorption presents a hydrogen bond between H in H_2O and O in MO_x clusters, which helps the adsorption of H_2O and renders the difference in adsorption energy. It is worthwhile to

note that the H_2O-induced stabilization of interfacial Sn is more significant than that for the Ce and Zn, showing a more downward shift for the states near the Fermi level and (Figures 10, S12 and S13). This is associated with the more drastic structural fluxionality of the SnO_2 cluster upon interaction with H_2O. Wherein the local structure of small SnO_2 cluster changes significantly to accommodate the $*H_2O$ and dissociation fragments (Figure 2), while much less was seen in the cases of CeO_2 and ZnO_2[29, 30]. With such unique structure, the SnO_2-Cu_2O interface can selectively suppress O_2 adsorption by the high-coordinated Sn sites and promote H_2O dissociative adsorption by the high structural fluxionality of SnO_2 cluster, which contributes to a higher $E_{ads}(O_2)/E_{ads}(H_2O)$ ratio and thus CH_3OH selectivity during CH_4 conversion by O_2 and H_2O.

3. Conclusions

With a combination of theoretical (DFT/KMC) and experimental (AP-XPS) studies, it was found that $SnO_2/Cu_2O/Cu(111)$ catalyst could achieve complete oxidation of CH_4 to CO_2 under a gas mixture of CH_4 and O_2 with a pressure ratio of 2:1 at 450K; with the addition of H_2O a 100% CH_3OH selectivity was observed, which was higher than the selectivity previously reported for $CeO_2/Cu_2O/Cu(111)$ and $ZnO/Cu_2O/Cu(111)$ surfaces. The complete selectivity tuning of from CO_2 to CH_3OH by introduction of H_2O reflects the unique atomic and electronic structure of highly dispersed SnO_2 nanoparticles at the SnO_2-$Cu_2O/Cu(111)$ interface. Specifically, the highly coordinated Sn cations at the interface can selectively suppress the adsorption of O_2, while the structural fluxionality of associated the SnO_2 species enables an enhancement in H_2O adsorption. Such selective binding properties ensure a high CH_3OH selectivity for CH_4 conversion on $SnO_2/Cu_2O/Cu(111)$.

4. Computational and Experimental Methods

4.1 DFT Calculations

Vienna *ab initio* simulation package (VASP)[48] was used to perform spin polarized density functional theory (DFT)[49, 50] calculations, where the setups for both geometry optimizations and transition state search followed those used in our previous studies[24, 30]. The dispersion forces were not considered here, since small differences (~1.1 kcal/mol) were reported previously for the reaction/activation energy of C-H bond breakage in CH_4 using the PBE XC functional with and without dispersion forces[23].

$SnO_2/Cu_2O/Cu(111)$ was modeled by depositing Sn_3O_6 clusters the over the 44 structure (Figure S1) as described previously[24]. According to the DFT-calculated phase diagram in our previous work[24], $Sn_3O_6/Cu_2O/Cu(111)$ is a major stable phase under the experimental conditions used for the preparation of the inverse catalysts. The size of the supported Sn_3O_6 cluster (~ 8 Å) matches very well with that measured experimentally (0.5~1.0 nm). Note that, as reported in preceding studies, the 44-structure, or $Cu_2O/Cu(111)$ in our notation, is critical to achieve a superior chemical activity over $Cu_2O(111)$, due to a strong $Cu_2O \leftrightarrow Cu$ interaction and a significant charge transfer from Cu to Cu_2O[37, 38, 51].

The adsorption energy was calculated as:

$$E_{ads} = E(\text{Ads/Surface}) - E(\text{Surface}) - E(\text{Ads})$$

where E is the DFT-calculated total energy including zero-point energy (ZPE) correction E_{ZPE}.

4.2 KMC Simulations

The KMC matrix was constructed in a way to well describe the dispersion of Sn_3O_6 smaller clusters on $Cu_2O/Cu(111)$ support as observed by STM (Figure S4). The reaction networks and input energies were based on the DFT results (Figures 1, 2 and 3 and Tables S1 and S2). Pressures in KMC simulations for CH_4, O_2, and H_2O were set as 100 Torr, 50 Torr and 400 Torr, respectively (see supporting information for details).

4.3 AP-XPS Measurements

The AP-XPS studies described above were carried out at beamline 9.3.2 at the Advanced Light Source (ALS), Lawrence Berkeley National Laboratory (LBNL) (see supporting information for details). The C 1s and O 1s data were collected using photon energies of 380 and 650 eV, respectively, with a total energy resolution of ~ 0.2 eV. For preparing the $SnO_2/Cu_2O/Cu(111)$ surfaces, we followed the methodology described in a previous article where the morphology was checked by STM (see Figure 1) and the Sn and Cu oxidation states were examined with XPS.[24]

Competing interests

The authors declare no competing interests.

Supporting Information

Details for methods used; Models used to describe $SnO_2/Cu_2O/Cu(111)$; DFT-optimized structures for reaction intermediates and transition states; Partial density of states; Parameters used for KMC simulations; KMC-simulated methane conversion and methanol production rate, KMC-simulated species concentrations.

Acknowledgements:

This work was performed at Brookhaven National Laboratory (BNL) thanks to the financial support of the division of Chemical Science, Geoscience, and Bioscience, Office of Basic Energy Science of the US Department of Energy (DOE contract No. DE-SC0012704). The theoretical calculations were carried out using computing clusters at Center for Functional Nanomaterials (CFN), and the Scientific Data and Computing Center, BNL, under Contract No. DE-SC0012704, at the National Energy Research Scientific Computing Center (NERSC), a U.S. DOE Office of Science User Facility located at Lawrence Berkeley National Laboratory (LBNL), supported by

the Office of Science of the U.S. DOE under Contract No. DE-AC02-05CH11231 using NERSC award BES-ERCAP0019897, at Stony Brook University, supported by National Science Foundation grant (#1531492). The XPS measurements were performed at beamline 9.3.2 at the Advanced Light Source (ALS), LBNL, a U.S. DOE Office of Science User Facility under contract DE-AC02-05CH11231. S.D.S. was supported by an Early Career Award by the U.S. DOE.

References:

1. Alvarez-Galvan, M. C.; Mota, N.; Ojeda, M.; Rojas, S.; Navarro, R. M.; Fierro, J. L. G., Direct methane conversion routes to chemicals and fuels. *Catal. Today* **2011,** *171* (1), 15-23.
2. Tang, P.; Zhu, Q.; Wu, Z.; Ma, D., Methane activation: the past and future. *Energy & Environmental Science* **2014,** *7* (8), 2580-2591.
3. Luo, L.; Luo, J.; Li, H.; Ren, F.; Zhang, Y.; Liu, A.; Li, W.-X.; Zeng, J., Water enables mild oxidation of methane to methanol on gold single-atom catalysts. *Nat. Commun.* **2021,** *12* (1), 1218.
4. Schwach, P.; Pan, X.; Bao, X., Direct Conversion of Methane to Value-Added Chemicals over Heterogeneous Catalysts: Challenges and Prospects. *Chem. Rev.* **2017,** *117* (13), 8497-8520.
5. Shaik, S.; Cohen, S.; de Visser, Samuël P.; Sharma, Pankaz K.; Kumar, D.; Kozuch, S.; Ogliaro, F.; Danovich, D., The "Rebound Controversy": An Overview and Theoretical Modeling of the Rebound Step in C−H Hydroxylation by Cytochrome P450. *Eur. J. Inorg. Chem.* **2004,** *2004* (2), 207-226.
6. Yoshizawa, K.; Shiota, Y.; Yamabe, T., Abstraction of the Hydrogen Atom of Methane by Iron−Oxo Species: The Concerted Reaction Path Is Energetically More Favorable. *Organometallics* **1998,** *17* (13), 2825-2831.
7. Olah, G. A., Beyond oil and gas: The methanol economy. *Angew. Chem. Int. Ed.* **2005,** *44* (18), 2636-2639.
8. Olah, G. A.; Prakash, G. K. S.; Goeppert, A., Anthropogenic Chemical Carbon Cycle for a Sustainable Future. *J. Am. Chem. Soc.* **2011,** *133* (33), 12881-12898.
9. Ravi, M.; Ranocchiari, M.; van Bokhoven, J. A., The direct catalytic oxidation of methane to methanol—A critical assessment. *Angew. Chem. Int. Ed.* **2017,** *56* (52), 16464-16483.
10. Khirsariya, P.; Mewada, R. K., Single step oxidation of methane to methanol–Towards better understanding. *Procedia Eng.* **2013,** *51*, 409-415.
11. Gesser, H. D.; Hunter, N. R.; Prakash, C. B., The direct conversion of methane to methanol by controlled oxidation. *Chem. Rev.* **1985,** *85* (4), 235-244.
12. Olivos-Suarez, A. I.; Szécsényi, À.; Hensen, E. J. M.; Ruiz-Martinez, J.; Pidko, E. A.; Gascon, J., Strategies for the Direct Catalytic Valorization of Methane Using Heterogeneous Catalysis: Challenges and Opportunities. *ACS Catalysis* **2016,** *6* (5), 2965-2981.
13. Sirajuddin, S.; Rosenzweig, A. C., Enzymatic oxidation of methane. *Biochemistry* **2015,** *54* (14), 2283-2294.

14. Wang, V. C. C.; Maji, S.; Chen, P. P. Y.; Lee, H. K.; Yu, S. S. F.; Chan, S. I., Alkane oxidation: Methane monooxygenases, related enzymes, and their biomimetics. *Chem. Rev.* **2017,** *117* (13), 8574-8621.
15. Chan, S. I.; Yu, S. S. F., Controlled oxidation of hydrocarbons by the membrane-bound methane monooxygenase: The case for a tricopper cluster. *Acc. Chem. Res.* **2008,** *41* (8), 969-979.
16. Shan, J.; Li, M.; Allard, L. F.; Lee, S.; Flytzani-Stephanopoulos, M., Mild oxidation of methane to methanol or acetic acid on supported isolated rhodium catalysts. *Nature* **2017,** *551*, 605-608.
17. Ross, M. O.; MacMillan, F.; Wang, J.; Nisthal, A.; Lawton, T. J.; Olafson, B. D.; Mayo, S. L.; Rosenzweig, A. C.; Hoffman, B. M., Particulate methane monooxygenase contains only mononuclear copper centers. *Science* **2019,** *364* (6440), 566-570.
18. Snyder, B. E. R.; Bols, M. L.; Schoonheydt, R. A.; Sels, B. F.; Solomon, E. I., Iron and copper active sites in zeolites and their correlation to metalloenzymes. *Chem. Rev.* **2018,** *118* (5), 2718-2768.
19. Newton, M. A.; Knorpp, A. J.; Sushkevich, V. L.; Palagin, D.; van Bokhoven, J. A., Active sites and mechanisms in the direct conversion of methane to methanol using Cu in zeolitic hosts: a critical examination. *Chem. Soc. Rev.* **2020,** *49* (5), 1449-1486.
20. Tomkins, P.; Ranocchiari, M.; van Bokhoven, J. A., Direct conversion of methane to methanol under mild conditions over Cu-zeolites and beyond. *Acc. Chem. Res.* **2017,** *50* (2), 418-425.
21. Sushkevich, V. L.; Palagin, D.; Ranocchiari, M.; van Bokhoven, J. A., Selective anaerobic oxidation of methane enables direct synthesis of methanol. *Science* **2017,** *356* (6337), 523-527.
22. Senanayake, S. D.; Rodriguez, J. A.; Weaver, J. F., Low temperature activation of methane on metal-oxides and complex interfaces: Insights from surface science. *Acc. Chem. Res.* **2020,** *53* (8), 1488-1497.
23. Liang, Z.; Li, T.; Kim, M.; Asthagiri, A.; Weaver, J. F., Low-temperature activation of methane on the IrO2(110) surface. *Science* **2017,** *356* (6335), 299-303.
24. Kang, J.; Rui, N.; Huang, E.; Tian, Y.; Mahapatra, M.; Rosales, R.; Orozco, I.; Shi, R.; Senanayake, S. D.; Liu, P.; Rodriguez, J. A., Surface characterization and methane activation on SnOx/Cu2O/Cu(111) inverse oxide/metal catalysts. *Physical Chemistry Chemical Physics* **2021,** *23* (32), 17186-17196.
25. Lustemberg, P. G.; Zhang, F.; Gutiérrez, R. A.; Ramírez, P. J.; Senanayake, S. D.; Rodriguez, J. A.; Ganduglia-Pirovano, M. V., Breaking Simple Scaling Relations through Metal–Oxide Interactions: Understanding Room-Temperature Activation of Methane on M/CeO2 (M = Pt, Ni, or Co) Interfaces. *J. Phys. Chem. Lett.* **2020,** *11* (21), 9131-9137.
26. Fung, V.; Tao, F.; Jiang, D.-e., Low-temperature activation of methane on doped single atoms: descriptor and prediction. *Phys. Chem. Chem. Phys.* **2018,** *20* (35), 22909-22914.
27. Lustemberg, P. G.; Palomino, R. M.; Gutierrez, R. A.; Grinter, D. C.; Vorokhta, M.; Liu, Z.; Ramirez, P. J.; Matolin, V.; Ganduglia-Pirovano, M. V.; Senanayake, S. D.; Rodriguez, J. A., Direct conversion of methane to methanol on Ni-Ceria surfaces: Metal-support interactions and water-enabled catalytic conversion by site blocking. *J. Am. Chem. Soc.* **2018,** *140* (24), 7681-7687.

28. Zuo, Z.; Ramírez, P. J.; Senanayake, S. D.; Liu, P.; Rodriguez, J. A., Low-Temperature Conversion of Methane to Methanol on CeOx/Cu2O Catalysts: Water Controlled Activation of the C–H Bond. *Journal of the American Chemical Society* **2016,** *138* (42), 13810-13813.
29. Liu, Z.; Huang, E.; Orozco, I.; Liao, W.; Palomino, R. M.; Rui, N.; Duchoň, T.; Nemšák, S.; Grinter, D. C.; Mahapatra, M.; Liu, P.; Rodriguez, J. A.; Senanayake, S. D., Water-promoted interfacial pathways in methane oxidation to methanol on a CeO2-Cu2O catalyst. *Science* **2020,** *368* (6490), 513-517.
30. Huang, E.; Orozco, I.; Ramirez, P. J.; Liu, Z.; Zhang, F.; Mahapatra, M.; Nemsak, S.; Senanayake, S. D.; Rodriguez, J. A.; Liu, P., Selective methane oxidation to methanol on ZnO/Cu2O/Cu(111) catalysts: Multiple site-dependent behaviors. *J. Am. Chem. Soc.* **2021,** *143* (45), 19018-19032.
31. Rodríguez, J. A.; Hrbek, J., Inverse oxide/metal catalysts: A versatile approach for activity tests and mechanistic studies. *Surf. Sci.* **2010,** *604* (3), 241-244.
32. Senanayake, S. D.; Stacchiola, D.; Rodriguez, J. A., Unique Properties of Ceria Nanoparticles Supported on Metals: Novel Inverse Ceria/Copper Catalysts for CO Oxidation and the Water-Gas Shift Reaction. *Accounts of Chemical Research* **2013,** *46* (8), 1702-1711.
33. Rodriguez, J. A.; Liu, P.; Graciani, J.; Senanayake, S. D.; Grinter, D. C.; Stacchiola, D.; Hrbek, J.; Fernández-Sanz, J., Inverse Oxide/Metal Catalysts in Fundamental Studies and Practical Applications: A Perspective of Recent Developments. *J. Phys. Chem. Lett.* **2016,** *7* (13), 2627-2639.
34. Rodriguez, J. A.; Grinter, D. C.; Liu, Z.; Palomino, R. M.; Senanayake, S. D., Ceria-based model catalysts: fundamental studies on the importance of the metal-ceria interface in CO oxidation, the water-gas shift, CO2 hydrogenation, and methane and alcohol reforming. *Chemical Society Reviews* **2017,** *46* (7), 1824-1841.
35. Rodriguez, J. A.; Graciani, J.; Evans, J.; Park, J. B.; Yang, F.; Stacchiola, D.; Senanayake, S. D.; Ma, S.; Pérez, M.; Liu, P.; Sanz, J. F.; Hrbek, J., Water-Gas Shift Reaction on a Highly Active Inverse CeOx/Cu(111) Catalyst: Unique Role of Ceria Nanoparticles. *Angew. Chem. Int. Ed.* **2009,** *48* (43), 8047-8050.
36. Orozco, I.; Huang, E.; Gutiérrez, R. A.; Liu, Z.; Zhang, F.; Mahapatra, M.; Kang, J.; Kersell, H.; Nemsak, S.; Ramírez, P. J.; Senanayake, S. D.; Liu, P.; Rodriguez, J. A., Hydroxylation of ZnO/Cu(1 1 1) inverse catalysts under ambient water vapor and the water–gas shift reaction. *J. Phys. D: Appl. Phys.* **2019,** *52* (45), 454001.
37. An, W.; Baber, A. E.; Xu, F.; Soldemo, M.; Weissenrieder, J.; Stacchiola, D.; Liu, P., Mechanistic Study of CO Titration on CuxO/Cu(1 1 1) (x⩽2) Surfaces. *ChemCatChem* **2014,** *6* (8), 2364-2372.
38. An, W.; Xu, F.; Stacchiola, D.; Liu, P., Potassium-Induced Effect on the Structure and Chemical Activity of the CuxO/Cu(111) (x <= 2) Surface: A Combined Scanning Tunneling Microscopy and Density Functional Theory Study. *Chemcatchem* **2015,** *7* (23), 3865-3872.
39. Waluyo, I.; Mudiyanselage, K.; Xu, F.; An, W.; Liu, P.; Boscoboinik, J. A.; Rodriguez, J. A.; Stacchiola, D. J., Potassium-Promoted Reduction of Cu2O/Cu(111) by CO. *The Journal of Physical Chemistry C* **2019,** *123* (13), 8057-8066.
40. Liao, W.; Liu, P., Methanol Synthesis from CO2 Hydrogenation over a Potassium-Promoted CuxO/Cu(111) (x ⩽ 2) Model Surface: Rationalizing the Potential of Potassium in Catalysis. *ACS Catal.* **2020**, 5723-5733.
41. Kattel, S.; Ramirez, P. J.; Chen, J. G.; Rodriguez, J. A.; Liu, P., Active sites for CO2 hydrogenation to methanol on Cu/ZnO catalysts. *Science* **2017,** *355* (6331), 1296-1299.

42. Kattel, S.; Liu, P.; Chen, J. G., Tuning selectivity of CO2 hydrogenation reactions at the metal/oxide interface. *J. Am. Chem. Soc.* **2017,** *139* (29), 9739-9754.
43. Senanayake, S. D.; Mudiyanselage, K.; Bruix, A.; Agnoli, S.; Hrbek, J.; Stacchiola, D.; Rodriguez, J. A., The Unique Properties of the Oxide-Metal Interface: Reaction of Ethanol on an Inverse Model CeOx-Au(111) Catalyst. *Journal of Physical Chemistry C* **2014,** *118* (43), 25057-25064.
44. Orozco, I.; Huang, E.; Mahapatra, M.; Shi, R.; Kang, J.; Nemšák, S.; Senanayake, S. D.; Liu, P.; Rodriguez, J. A., In Situ Studies of Methanol Decomposition Over Cu(111) and Cu2O/Cu(111): Effects of Reactant Pressure, Surface Morphology, and Hot Spots of Active Sites. *J. Phys. Chem. C* **2020,** *125* (1), 558-571.
45. Batzill, M., Surface Science Studies of Gas Sensing Materials: SnO2. *Sensors* **2006,** *6* (10), 1345-1366.
46. Kulkarni, A. R.; Zhao, Z. J.; Siahrostami, S.; Norskov, J. K.; Studt, F., Cation-exchanged zeolites for the selective oxidation of methane to methanol. *Catal. Sci. Technol.* **2018,** *8* (1), 114-123.
47. Mahapatra, M.; Kang, J. D.; Ramiirez, P. J.; Hamlyn, R.; Rui, N.; Liu, Z. Y.; Orozco, I.; Senanayake, S. D.; Rodriguez, J. A., Growth, structure, and catalytic properties of ZnOx grown on CuOx/Cu(111) surfaces. *J. Phys. Chem. C* **2018,** *122* (46), 26554-26562.
48. Kresse, G.; Furthmuller, J., Efficient iterative schemes for ab initio total-energy calculations using a plane-wave basis set. *Phys. Rev. B* **1996,** *54* (16), 11169-11186.
49. Hohenberg, P.; Kohn, W., Inhomogeneous electron gas. *Phys. Rev.* **1964,** *136* (3B), B864-B871.
50. Kohn, W.; Sham, L. J., Self-consistent equations including exchange and correlation effects. *Phys. Rev.* **1965,** *140* (4A), A1133-A1138.
51. Mudiyanselage, K.; An, W.; Yang, F.; Liu, P.; Stacchiola, D. J., Selective molecular adsorption in sub-nanometer cages of a Cu2O surface oxide. *Phys. Chem. Chem. Phys.* **2013,** *15* (26), 10726-10731.

For Table of Contents Only